

## UWB MICROWAVE IMAGING FOR BREAST CANCER DETECTION — EXPERIMENTS WITH HETEROGENEOUS BREAST PHANTOMS

J. C. Y. Lai, C. B. Soh, E. Gunawan, and K. S. Low

School of Electrical and Electronic Engineering  
Nanyang Technological University  
50 Nanyang Avenue, Singapore 639798, Singapore

**Abstract**—The paper describes pulse-based ultra-wideband (UWB) radar microwave imaging experiments for breast cancer detection using breast phantoms with dielectric properties mimicking the human breast. Three homogeneous and seven heterogeneous breast phantoms are designed with a series of dielectric permittivity and variability and are used in tumor detection experiments. The experiments are conducted in time-domain with pulse generator and real-time oscilloscope.

### 1. INTRODUCTION

Ultra-wideband (UWB) microwave imaging for breast cancer detection has attracted research interest with the prospect of replacing X-ray mammography as the screening tool for early breast cancer detection [1, 2]. The potential of UWB for breast cancer detection has been demonstrated with experiments on simple homogenous breast phantoms, where soy bean oil [3] and flour-oil-saline mixture [4] have been used to simulate breast tissue in UWB imaging experiments. Successful detection of tumor simulants of 4 mm and 10 mm diameter are reported in the respective experiments.

However, the dielectric permittivity and dielectric loss of the above mentioned materials are much lower than human breast. The reported experiments simulate only the dielectric contrast between malignant and normal breast tissue, where loss factors when the signals propagate through the breast medium are ignored. Furthermore, the breast

phantom materials are unable to simulate the heterogeneous nature of human breast in stable solid form.

Recently, more realistic breast phantoms with dielectric permittivity and dielectric loss close to the human breast have been reported in the literature. Salvador and Vecchi [5] presented experiments using high dielectric homogeneous breast phantom made of flour-water mixture and coupling medium of alcohol. Klemn et al. [6] reported the first experiments conducted with inhomogeneous breast phantom designed with dense tissue made of polythene powder and water mixture at the center of the breast. Though the breast phantom is more anatomically realistic, the tumor is placed outside the dense tissue and thus does not pose a challenge for detection. The materials used to simulate breast and tumor tissues in published experimental studies are summarized in Table 1.

The aim of this paper is to conduct UWB imaging experiments with a series of homogeneous and heterogeneous breast phantoms with a range of dielectric permittivity and variability. The paper gives a better understanding of the requirements for the development of a practical UWB microwave imaging screening tool for early breast cancer detection.

The experiments were conducted in time domain which is more technically challenging since the power spectrum of the signal is limited by the pulse generated, whereas in frequency domain, the full spectrum across the UWB frequencies can be used. Furthermore, time domain measurement can leverage on the advances in UWB communication technologies such as wireless USB and body area network.

**Table 1.** Dielectric permittivity of the tissues simulating materials and tumor size used in reported UWB microwave imaging experiments.

Experiment	Li et al. [3]	Sill et al. [4]	Salvador et al. [5]	Klemn et al. [6]
Frequency †	6 GHz	4 GHz	1 GHz	3 GHz
Low dielectric Adipose tissue	2.6	4.2	N.A	10
High dielectric Glandular tissue	N.A.	N.A.	48	20–30
Skin	4.3	34	N.A.	35
Tumor	8.7	44	80	50
Tumor Size	4 mm	10 mm	10 mm	10 mm

† is the frequency at which the dielectric permittivity was reported; in all experiments, ultra-wideband frequencies are used in imaging of breast tumor.

## 2. METHODS AND EXPERIMENTAL SETUP

In this paper, breast phantoms are fabricated using tissue mimicking phantom material consists of oil-in-gelatin dispersions proposed by Lazebnik et al. [7]. Phantom materials with different concentration of oil are used to construct breast phantoms of different dielectric permittivity, in plastic containers of 10 cm diameter and 8 cm height.

Three homogeneous and seven heterogeneous breast phantoms are fabricated by mixing phantom materials made of different volumes of oil. Clutters in the breast are made of material with low percentage of oil to simulate the glandular tissue, whereas matrix to hold the clutters is made of material with high percentage of oil to simulate the adipose tissue. Clutters are prepared by mincing the high dielectric phantom material to size smaller than 5 mm and are randomly distributed in the breast.

The details of breast phantoms fabrication and dielectric properties measurement are presented in [8]. The dielectric permittivity and variability of the fabricated homogeneous and heterogeneous breast phantoms are given in Table 2. For heterogeneous breast phantoms, variability is calculated with the range divided by two times the mean dielectric permittivity, where the range of dielectric permittivity is the difference between dielectric permittivity of clutters and matrix materials.

Phantoms Hetero-17, Hetero-25, Hetero-33, and Hetero-50 are fabricated by fixing the clutters dielectric permittivity and varying the

**Table 2.** Three homogeneous and seven heterogeneous breast phantoms used in UWB imaging experiments.

Breast Phantom	% of oil in clutters	% of clutters in phantom	Dielectric Permittivity	Dielectric Variability
Homo-80	-	0%	8	0%
Homo-65	-	0%	16	0%
Homo-50	-	0%	24	0%
Hetero-17	50%	17%	10	$\pm 80\%$
Hetero-25	50%	25%	11	$\pm 73\%$
Hetero-33	50%	33%	13	$\pm 62\%$
Hetero-50	50%	50%	16	$\pm 50\%$
Hetero-70	70%	50%	10	$\pm 46\%$
Hetero-65	65%	50%	11	$\pm 36\%$
Hetero-60	60%	50%	13	$\pm 20\%$

percentage of clutters to simulate different volumes of glandular and fibroconnective tissues. Phantoms Hetero-70, Hetero-65, and Hetero-60 are fabricated by fixing percentage of clutters and varying the clutters dielectric permittivity to simulate different breast dielectric properties.

Tumor simulants in cylindrical shape of 10 mm length, with 2 mm and 4 mm diameter, are made of tissue mimicking phantom material with 10% oil. The dielectric constant at 5 GHz for tumor simulant is 50, which is representative of malignant breast tissue. The simulant is inserted into the breast phantoms at depth of 4 cm from top and 2 cm from the central axis.

Figures 1 and 2 summarize the experiments done in this study as compared to published results. From Lazebnik's [9] large scale study, the dielectric permittivity of normal breast tissue is in the range of 4 to 48. The median dielectric permittivity is 34 and the range of dielectric constant is approximately 44 with variability of  $\pm 65\%$ . The variability is much higher than the commonly assumed value of  $\pm 10\%$  in simulation studies.

The overall experimental setup is shown in Figure 3 with transmitter and receiver antennas in bistatic configuration. Breast phantom is placed on a rotary stage with antennas scanning at the side to simulate the human breast in prone position. Breast phantom

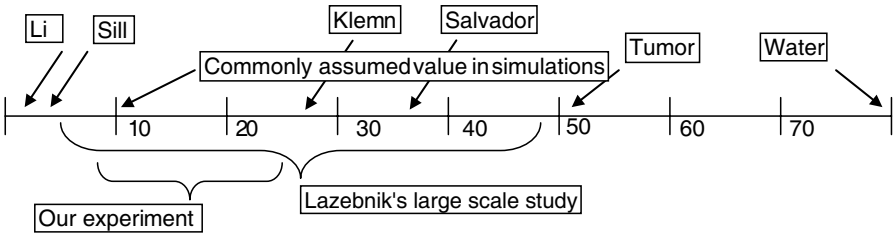


**Figure 1.** Dielectric constant of breast tissue.

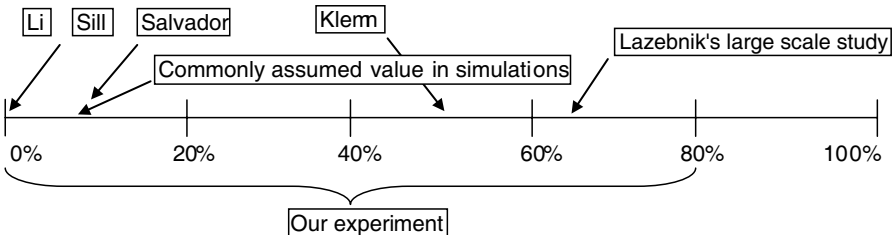


**Figure 2.** Variability of breast tissues dielectric constant.

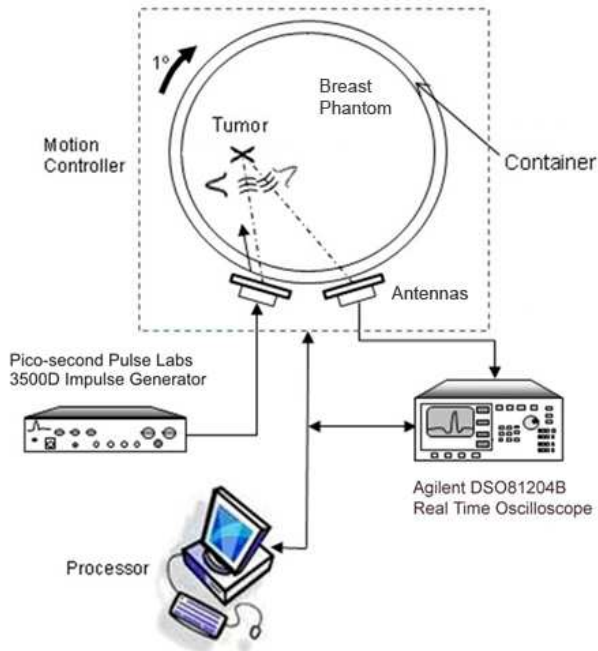


**Figure 3.** Overall experimental setup.

is rotated for 360 degrees relative to the stationary antennas to simulate a circular array of 360 antennas around the breast circumference.

The excitation signal is generated using the Picosecond Pulse Labs 3500D impulse generator, which produces gaussian pulses with full width at half maximum (FWHM) of 80 picoseconds. Agilent DSO81204B real-time oscilloscope with 40 GHz sampling rate is used for recording the backscattered signals from the breast phantom.

Thales UWB antennas [10] are used as the transmitter and receiver of the UWB signals. The antennas dimension is 3 cm width and 4 cm height. The antennas gain is 11 dB with azimuth beamwidth of 60 degrees and elevation beamwidth of 40 degrees. The antennas return loss is lower than  $-10$  dB from 2.4 to 12 GHz.

Before processing of the collected signals, calibration is performed to remove the early time artifact [2], which includes incident pulse, boundary reflection and multipath. In the paper, two calibration approaches are implemented to compare the results. Subtraction method is applied by subtracting the data from tumor-free phantom

with data from tumor-bearing phantom, whereas averaging method is applied by subtracting the average of all received signals with signal from individual antenna [1].

Delay-and-sum beamforming [1] algorithm is used to generate the image as in confocal imaging technique. Cross-sectional image of the cylindrical breast phantom is formed by synthetically focusing the signals received from the antenna array to every point within the scanning plane. The final image formed is an intensity image indicating the location of microwave scatterers.

### 3. RESULTS AND DISCUSSIONS

Imaging results for three homogeneous breast phantoms, named Homo-50, Homo-65, and Homo-80, are shown in Figure 4, whereas the seven heterogeneous breast phantoms, named Hetero-17, Hetero-25, Hetero-33, Hetero-50, Hetero-60, Hetero-65, and Hetero-70, are shown in Figure 5. The names for 17, 25, 33, and 50 indicate the percentage of clutters used in fabrication, with clutters made of 50% of oil. The

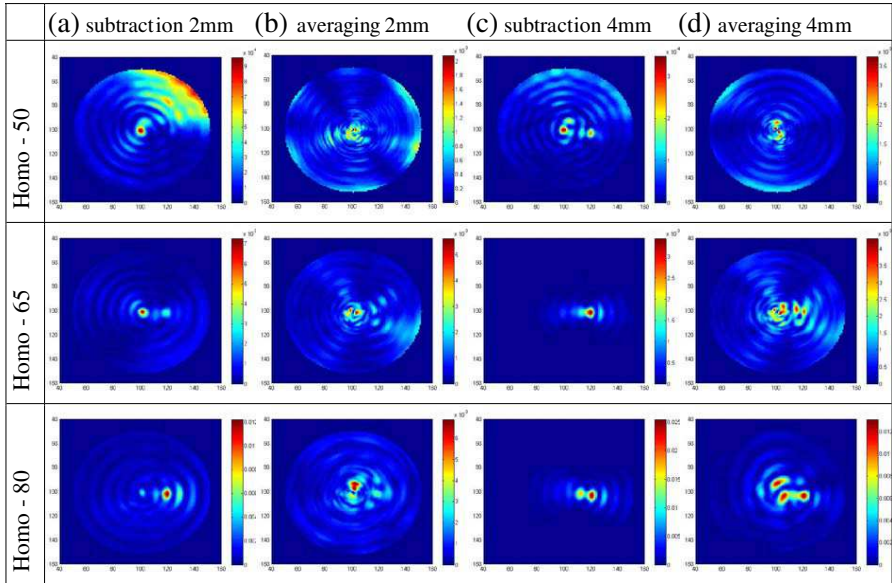


**Figure 4.** Imaging results for homogeneous breast phantoms Homo-50, Homo-65, and Homo-80 (a) 2 mm tumor with subtraction method, (b) 2 mm tumor with averaging method, (c) 4 mm tumor with subtraction method, (d) 4 mm tumor with averaging method.

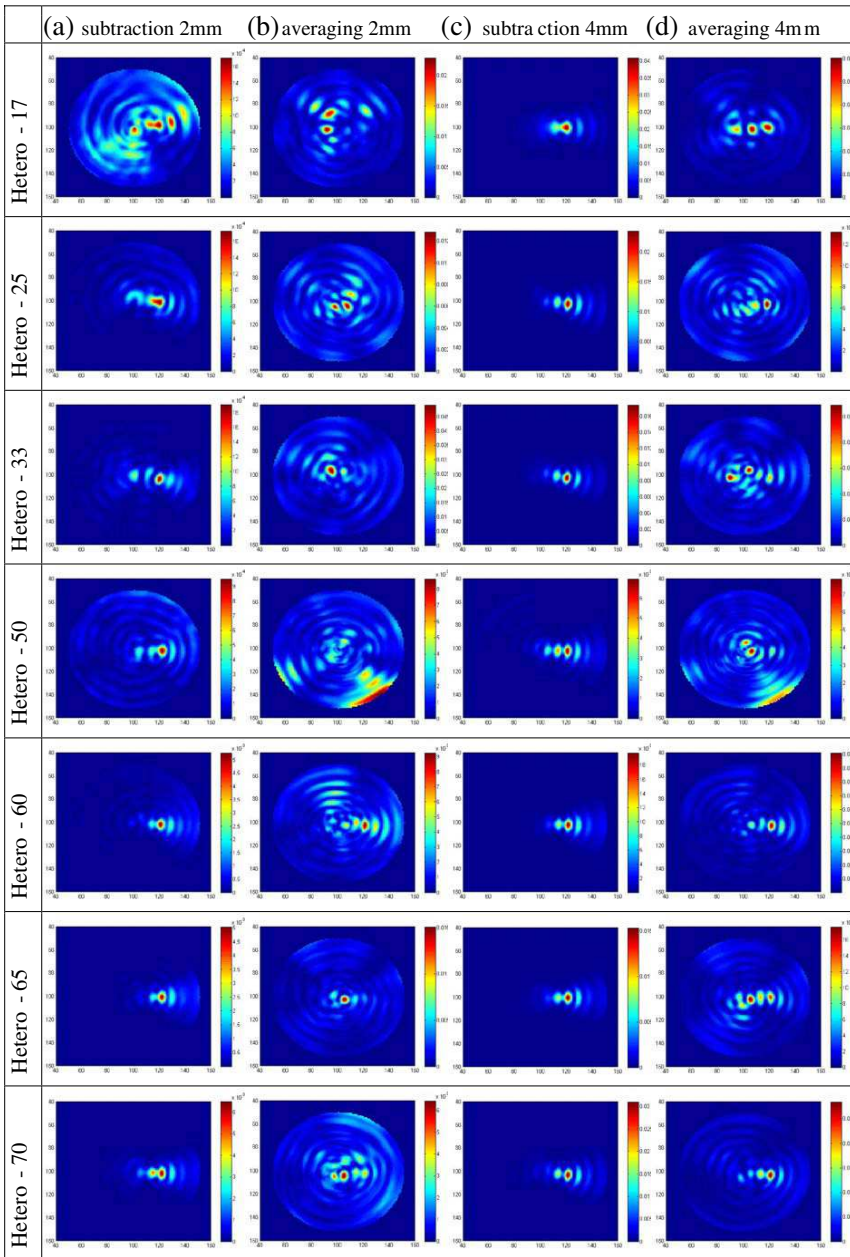
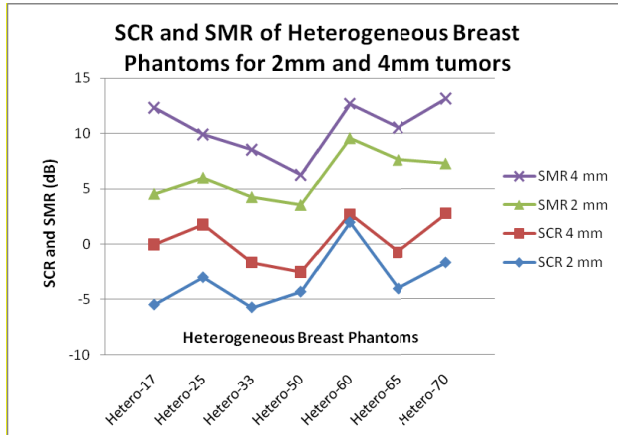


Figure 5. Imaging results for seven homogeneous breast phantoms.



**Figure 6.** SCR and SMR for heterogeneous breast phantoms.

names for 60, 65, and 70 indicate the percentage of oil in clutters used in fabrication, with 50% of clutters. Images formed with subtraction method of artifact removal are the left figures to be compared to the right figures formed with averaging method.

With subtraction method of artifact removal, tumor was successfully detected in most of the breast phantoms, except breast phantom Homo-50, which the signal loss is severe in the medium with averaged dielectric permittivity of 24 and conductivity of 3.2S/m. For all heterogeneous breast phantoms, the signals reflected by the small tumor amidst the heterogeneous breast clutters are within the detection ability of the experimental setup. With averaging method, 4 mm tumor could be detected only in half of the phantoms, and 2 mm tumor could not be detected in most of the breast phantoms. This is reasonable since the clutters prepared have random size from 0.5 to 5 mm.

Signal-to-Clutter and Signal-to-Mean ratios of all the breast images are given in Table 3 for both subtraction and averaging methods. The ratios for homogeneous and heterogeneous breast phantoms are plotted in Figures 6 and 7 respectively. It is clear from the plots that the major hindrance to successful detection of tumor is signal attenuation due to high dielectric permittivity of the breast tissues, whereas the dielectric variability does not show much correlation with the Tumor-to-Clutter ratio. For reference, the dynamic range of oscilloscope in the experimental setup is 72 dB (12 bits).

**Table 3.** Signal-to-Clutter ratio (SCR) and Signal-to-Mean ratio (SMR) of breast images formed by subtraction and averaging methods.

Phantom	Subtraction				Averaging			
	2 mm tumor		4 mm tumor		2 mm tumor		4 mm tumor	
	SCR	SMR	SCR	SMR	SCR	SMR	SCR	SMR
Homo-50	-4.79	2.89	-1.19	9.06	-6.32	2.19	-7.67	1.85
Homo-65	-3.54	9.32	4.18	17.69	-3.59	6.60	-0.62	8.86
Homo-80	2.99	12.30	1.63	16.43	-3.11	6.87	0.23	11.88
Hetero-17	0.34	7.25	2.79	17.33	-5.48	4.53	-0.02	12.31
Hetero-25	3.40	13.38	3.41	18.10	-3.00	5.99	1.74	9.89
Hetero-33	2.64	14.26	3.01	18.19	-5.73	4.24	-1.66	8.51
Hetero-50	3.53	11.44	2.53	16.05	-4.31	3.52	-2.50	6.25
Hetero-60	3.36	15.22	3.37	17.84	1.99	9.59	2.70	12.69
Hetero-65	3.61	16.59	3.70	17.78	-4.03	7.60	-0.76	10.51
Hetero-70	3.59	16.75	3.72	17.47	-1.69	7.25	2.75	13.15

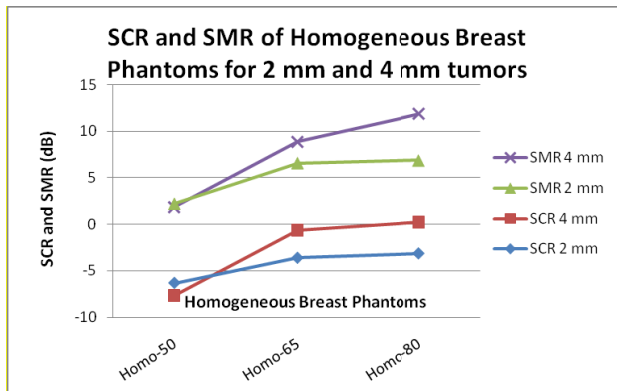


**Figure 7.** SCR and SMR for homogeneous breast phantoms.

An important conclusion from the results is that hardware is the major limitation to detect small tumor in breast with higher dielectric permittivity, whereas software would determine the successful tumor detection in heterogeneous breast. In this respect, more advanced algorithms could be used to reduce the artifacts in the received signals, as well as clutters responses for the heterogeneous breast phantoms. Methods based on eliminating coherent components in the received signals, such as averaging method, would not provide successful results because clutters responses are non-coherent from different antennas,

and thus cannot be eliminated.

It is worth nothing that although there are many more complex algorithms available in the literature, the algorithms may not be useful in practice. Most of the algorithms which claim to enhance the tumor response are in fact enhancing only the image contrast. In cases where the tumor is not the strongest microwave scatterer in the breast, these algorithms will produce worse results by enhancing other clutter responses, as has been shown in [11]. Thus we anticipate algorithm which is able to differentiate the characteristic of tumor and clutters responses is needed for successful detection of breast cancer in realistic heterogeneous breast medium.

#### 4. CONCLUSION

In the paper, we have conducted experiments with three homogeneous and seven heterogeneous breast phantoms with a series of dielectric permittivity and variability. The experiments have been done in time domain using pulse generator and real-time oscilloscope. The experiment shows that hardware limitation is the major factor for detecting millimeter size breast tumor in breast phantoms with higher dielectric permittivity, whereas software limitation would determine the successful detection of tumor in heterogeneous breast medium.

#### REFERENCES

1. Li, X. and S. C. Hagness, "A confocal microwave imaging algorithm for breast cancer detection," *IEEE Microwave and Wireless Components Letters*, Vol. 11, No. 3, 130–132, Mar. 2001.
2. Fear, E. C., S. C. Hagness, P. M. Meaney, M. Okoniewski, and M. A. Stuchly, "Enhancing breast tumor detection with near-field imaging," *IEEE Microwave Magazine*, Vol. 3, 48–56, Mar. 2002.
3. Li, X., S. K. Davis, S. C. Hagness, D. W. van der Weide, and B. D. van Veen, "Microwave imaging via space-time beamforming: Experimental investigation of tumor detection in multi-layer breast phantoms," *IEEE Transactions on Microwave Theory and Techniques*, Vol. 52, No. 8, 1856–1865, Aug. 2004.
4. Sill, J. M. and E. C. Fear, "Tissue sensing adaptive radar for breast cancer detection — Experimental investigation of simple tumor models," *IEEE Transactions on Microwave Theory and Techniques*, Vol. 53, No. 11, 3312–3319, Nov. 2005.
5. Salvador, S. M. and G. Vecchi, "Experimental tests of microwave

- breast cancer detection on phantoms,” *IEEE Transactions on Antennas and Propagation*, Vol. 57, No. 6, 1705–1712, Jun. 2009.
6. Klemm, M., J. A. Leendertz, D. Gibbins, I. J. Craddock, A. Preece, and R. Benjamin, “Microwave radar-based breast cancer detection: Imaging in inhomogeneous breast phantoms,” *IEEE Antennas and Wireless Propagation Letters*, Vol. 8, 1349–1352, 2009.
  7. Lazebnik, M., E. L. Madsen, G. R. Frank, and S. C. Hagness, “Tissue-mimicking phantom materials for narrowband and ultrawideband microwave applications,” *Physics in Medicine and Biology*, Vol. 50, 4245–4258, 2005.
  8. Lai, J. C. Y., C. B. Soh, E. Gunawan, and K. S. Low, “Homogeneous and heterogeneous breast phantoms for ultra-wideband microwave imaging applications,” *Progress In Electromagnetics Research*, Vol. 100, 397–415, 2010.
  9. Lazebnik, M., L. McCartney, D. Popovic, C. B. Watkins, M. J. Lindstrom, J. Harter, S. Sewall, A. Magliocco, J. H. Booske, M. Okoniewski, and S. C. Hagness, “A large-scale study of the ultrawideband microwave dielectric properties of normal breast tissue obtained from reduction surgeries,” *Physics in Medicine and Biology*, Vol. 52, 2637–2656, May 2007.
  10. Chua, L. W., “A new UWB antenna with excellent time domain characteristics,” *Proc. The European Conference on Wireless Technology*, 531–534, Oct. 2005.
  11. O’Halloran, M., M. Glavin, and E. Jones, “Effects of fibroglandular tissue distribution on data-independent beamforming algorithms,” *Progress In Electromagnetics Research*, Vol. 97, 141–158, 2009.